HHS Public Access

Author manuscript

J Neuroimaging. Author manuscript; available in PMC 2023 November 10.

Published in final edited form as:

J Neuroimaging. 2019 November ; 29(6): 760–770. doi:10.1111/jon.12654.

Effects of Optic Neuritis, T2 Lesions, and Microstructural Diffusion Integrity in the Visual Pathway on Cortical Thickness in Pediatric-Onset Multiple Sclerosis

Ritobrato Datta,

John R. Sollee,

Amy M. Lavery,

Gabriella Ficerai-Garland,

Krystle Karoscik,

Geraldine Liu,

Brenda L. Banwell,

Amy T. Waldman

Division of Neurology, Department of Pediatrics, Children's Hospital of Philadelphia, Philadelphia, PA (RD, JRS, AML, GFG, KK, GL, BLB, ATW); Departments of Neurology and Pediatrics, Perelman School of Medicine at the University of Pennsylvania, Philadelphia, PA (BLB, ATW).

Abstract

BACKGROUND AND PURPOSE: Pediatric-onset multiple sclerosis (POMS) is associated with focal inflammatory lesions and the loss of cortical and deep gray matter. Optic neuritis (ON) and white matter (WM) lesions in the visual pathway can directly contribute to visual cortical mantle thinning. We determine the relative contributions of MS insult on anterior and posterior visual pathway integrity.

METHODS: High- and low-contrast visual acuity, optical coherence tomography (OCT), and 3T MRI scans were obtained from 20 POMS patients (10 with remote ON) and 22 age- and sex-matched healthy controls. Cortical mantle thickness was measured using FreeSurfer. Fractional anisotropy (FA) and mean diffusivity were calculated for postchiasmal optic radiations (with and without WM lesions). Groups were compared using Student's *t*-test (adjusted for multiple comparisons), and simple linear regression was used to investigate interrelationships between measures.

RESULTS: Mean cortical thickness of the whole brain was reduced in patients (2.49 mm) versus controls (2.58 mm, $P = .0432$) and in the visual cortex (2.07 mm vs. 2.17 mm, $P = .0059$), although the foveal confluence was spared. Mean FA of the optic radiations was reduced in POMS (.40) versus controls (.43, $P = .0042$) and correlated with visual cortical mantle thickness in POMS ($P = .017$). Visual acuity, OCT measures, and lesion volumes in the optic radiations were not associated with cortical mantle thickness.

Correspondence: Address correspondence to Amy T. Waldman, MD, MSCE, Division of Neurology, Department of Pediatrics, Children's Hospital of Philadelphia, CTRB, 10th Floor, Room 10012, 3401 Civic Center Boulevard, Philadelphia, PA 19104. waldman@email.chop.edu.

CONCLUSIONS: POMS negatively impacts the integrity of the anterior visual pathway, but it is the loss of WM integrity that drives anterograde loss of the cortical mantle. Preserved visual acuity and foveal sparing imply some degree of functional and structural resilience.

Keywords

Multiple sclerosis; pediatrics; optical coherence tomography; diffusion tensor imaging; magnetic resonance imaging

Introduction

Optic neuritis (ON) is a common feature of adult- and pediatric-onset multiple sclerosis (POMS). Inflammatory damage of the optic nerves leads to retrograde retinal atrophy, as measured by thinning of the retinal nerve fiber (RNFL) and ganglion cell layer-inner plexiform layer (GCL-IPL).[1–3] This axonal loss in the afferent visual pathway could also lead to anterograde reduction in neuronal density, quantifiable as a reduction in visual cortical mantle thickness, as has been documented in adults with MS.[4–6] Loss of cortical volume may also be a consequence of intracortical lesions and neuronal loss.[7–10]

We quantify cortical mantle thickness in primary and secondary visual areas in POMS, first to determine whether young MS patients experience measurable insult to the cortex early in their disease. Recognizing that ON clearly impacts the anterior pathway, we deliberately compared POMS patients with and without a history of ON to determine whether this clear anterograde insult would be even more likely to impact downstream visual pathway integrity. Given that POMS patients also accrue a high lesion burden in the white matter (WM),[11] we evaluated whether T2 bright focal lesions in the visual pathway impacted visual cortical mantle thickness. Finally, we performed diffusion tensor imaging (DTI) to evaluate the integrity of occipital WM pathways. The interrelationships between all of these anterior and posterior visual pathway metrics were then determined.

Methods

Participants

Consecutive patients with relapsing-remitting POMS, as defined by the 2010 McDonald criteria,[12] and whose age at first attack was <18 years were recruited from the Pediatric MS Program at the Children's Hospital of Philadelphia. A history of ON was confirmed based on visual impairment lasting at least 24 hours, associated with one or more of pain with ocular movement, color perception desaturation, enlarged central scotoma, or optic disc swelling.[13] All participants were enrolled at least 6 months following ON or corticosteroid treatment for any MS relapse. For each POMS participant, disease duration (time from first attack), annualized relapse rate, and Expanded Disability Status Scale (EDSS) score were determined. Participants were excluded if they had a neuroinflammatory diagnosis other than POMS. Healthy controls (HC) without neurologic or ophthalmologic disease were recruited by local advertisement. For both groups, participants were excluded if they had dental hardware. The study was approved by the Children's Hospital of Philadelphia

Institutional Review Board. Written informed consent was provided by all participants, and child assent was obtained.

Visual acuity was measured at a distance of 2 m using high-contrast visual acuity (HCVA; Early Treatment Diabetic Retinopathy Study [ETDRS], Precision Vision, Woodstock, IL) and low-contrast letter acuity (LCLA; Sloan 2.5% and 1.25%, Precision Vision) charts with an illuminator cabinet in a dark room. All charts contained five letters per line, with a maximum score of 70 letters corresponding to a Snellen equivalent of 20/10.

Spectral domain optical coherence tomography (OCT) was obtained in a dark room without windows by a single trained technician using Cirrus HD-OCT (Model 5000, software version 6.5; Carl Zeiss Meditec, Inc., Dublin, CA) at 27,000 A-scans/second. Participants underwent the Optic Disc Cube (200 × 200 scans) and Macular Cube (512 × 128) protocols for each undilated eye while fixating on landmarks positioned nasally or centrally to the Optic Disc Cube and Macular Cube, respectively. The technician verified that the images were focused and centered with uniform illumination and assessed for artifacts, as recommended by the OSCAR-IB Consensus Criteria for Retinal OCT Quality Assessment.[14] Only scans meeting these criteria and having a signal strength ≥7 were used for the analysis. Segmentation was performed using the built-in automatic segmentation algorithm of the OCT system. Inspection of the resulting Macular Cube cross sections revealed no evidence for eccentric fixation, as the fovea was always centered at fixation.

MRI Acquisition

All participants were scanned on the same 3T scanner (Siemens, Verio, Orem, UT) with a Siemens 32-channel head coil. Anatomical images were acquired using a standard T1-weighted high-resolution anatomical scan using Fast Low Angle Shot (FLASH; 192 slices, 1 mm isotropic, repetition time (TR) = 20 ms, echo time (TE) = 5 ms, field of view (FOV) = 256 mm, flip angle = 27°) and 3D FLAIR (208 slices, 1 mm isotropic, TR = 5,000 ms, TE = 388 ms, FOV = 256 mm) acquisitions. DTI images were recorded using a 2D echo-planar imaging sequence with diffusion weighting in 64 directions and *b*-value of 1,000 s/mm^2 (TR = 10,300 ms, TE = 95 ms, FOV = 256 mm, number of slices = 50, voxel size = 2.0 mm isotropic).

MRI Analysis

All images from each participant were visually inspected to ensure the images were devoid of motion artifact and signal dropouts in the different regions. FreeSurfer toolkit (https://surfer.nmr.mgh.harvard.edu, version 6) was used to segment each T1 FLASH image. Pial (gray matter [GM]/cerebrospinal fluid, ie, outer boundary of cortical mantle) and GM/WM (ie, inner boundary of cortical mantle) surfaces were reconstructed.[15] A quality check was performed on each subject's processed data by manually examining each slice to ensure accurate GM and WM segmentation. Lesions that disturbed the cortex segmentation were accounted for by manual correction of WM topology (ie, adding voxels of these lesions to WM volume, referred to as filling), and the pipeline was rerun. For regions with segmentation errors, control points were added manually to indicate WM voxels that were erroneously classified as GM. As per methods in FreeSurfer, these voxels were normalized

to a value of 110, the standard for WM. The data were rechecked to ensure segmentation accuracy. Cortical thickness was then estimated at each point across the cortical mantle by calculating the distance between the GM/WM boundary and the pial boundary. Cortical mantle thickness was compared in a priori selected regions of interest (ROIs). The cortical mantle in the right and left hemispheres was subdivided into different ROIs corresponding to the different retinotopic visual areas (V1–V3) in the medial visual cortex using cortical surface topology templates;[16] subregions of the dorsolateral visual cortex[17] and the ventral visual regions comprising of hV4, ventral occipital areas 1–2, parahippocampal cortex areas 1–2, and fusiform gyrus (FG) areas 2–4 were also considered.[18] This method of cortical surface alignment using gyral landmarks allows for accurate prediction not only of the boundaries of the different visual areas but also the assignment of retinotopic polar angle and eccentricity co-ordinates onto the visual cortex.[16] We utilized a surface-based retinotopic eccentricity template to define the cortical region of the occipital lobe subtending 2 degrees of visual angle of central vision, termed the foveal confluence.[16,19] In addition to measuring the cortical thicknesses of the predefined ROIs in each hemisphere, mean of left and right hemisphere ROIs, whole cortex, and whole hemisphere average thickness measures were calculated.

DTI processing was conducted using FMRIB Software Library (FSL) tools (www.fmrib.ox.ac.uk/fsl/). DTI data were corrected for MRI eddy currents and head motion using affine registration to a reference volume ($b = 0$). Then, images were brain extracted using brain extraction tool, and a diffusion tensor model was fit at each voxel. For each subject, fractional anisotropy (FA) and mean diffusivity (MD) maps were generated on a voxel-wise level. Mean FA and MD values were computed for optic radiations excluding the lesions and for the lesions within the optic radiations in the POMS group.

Identifying Lesional and Nonlesional Tissue

Lesion Segmentation Toolbox (lesion growth algorithm: https://www.applied-statistics.de/lst.html) was used to identify T2 lesions using FLAIR and T1 images. Total T2 lesion volume of the whole brain and the T2 lesion volume within the optic radiations were calculated from the lesion probability maps. Optic radiations were demarcated using the Juelich Histological Atlas optic radiation probability map. Each subject's brain was nonlinearly registered to the MNI template using advanced normalization tools. The optic radiation mask (part of Juelich Histological Atlas) at a threshold of 25% was warped to the subject's native space using an inverse transformation. All non-WM voxels were removed using segmentations available in FreeSurfer. The DTI data obtained in the same session were registered to the T1 image using linear registration. The optic radiation mask was then resampled to the DTI space using the nearest neighbor interpolation. Each mask was manually checked for accuracy.

Statistical Analysis

Demographic, visual acuity, and OCT variables were compared using the Student's *t*-test for independent samples. Cortical thickness and DTI measures were adjusted for the effects of age and sex using a general linear model. After fitting, the residual data from this model was taken as the adjusted measure and used for subsequent analyses using the Student's

t-test for independent samples to identify whether the cortical thickness and DTI measures differed between POMS and HC; the false discovery rate was used to adjust for multiple comparisons, and Benjamini-Hochberg *P*-values were computed. The POMS group was also stratified by ON history, and the Student's *t*-test for independent samples was used to compare demographic and anatomical measures between POMS-ON, POMS non-ON, and HC groups. Simple linear regression was used to investigate the interrelationships between measures. All statistical analyses were performed using Stata Statistical Software (version 12.1; StataCorp LP, College Station, TX).

Results

Demographics and Clinical Features

Twenty subjects with POMS and 22 HCs were enrolled. Demographic and clinical features are presented in Table 1. Comparing POMS subjects with remote ON to those POMS subjects without a clinical history of ON, there were no differences in age, sex, annualized relapse rate, disease duration, or treatment duration (all $P > .28$, data not shown). The mean binocular HCVA and LCLA (2.5%) scores did not differ between POMS and HCs (Table 2); however, binocular LCLA (1.25%) scores were, on average, six-letters lower in the POMS group ($P = .0387$), which represents a greater than one-line deficit in Snellen acuity. Binocular LCLA (1.25%) scores for POMS-ON subjects (mean 20 letters [SD 10.9]) did not differ from POMS non-ON subjects (mean 22.1 letters [SD 10.0], $P = .6582$).

OCT Measures

Mean RNFL thickness (averaged between the right and left eyes) was reduced in POMS patients ($P = .0480$, Table 2); however, the relationship was driven by ON eyes, which contributed to a decreased average RNFL thickness in POMS-ON subjects (mean RNFL: 81.3 μm [SD 10.7]), which was significantly thinner compared to POMS non-ON subjects (100.1 μm [SD 10.0], $P = .0007$). Mean GCL-IPL (averaged between the right and left eye) thickness was also reduced in POMS subjects ($P = .0107$, Table 2), with greater thinning again in POMS-ON subjects (mean GCL-IPL 72 μm [SD 7.4]), compared to POMS non-ON subjects (79.4 μm [SD 8.3]), although this did not reach significance ($P = .0680$).

Cortical Thickness

The average cortical mantle thickness for the cerebral cortex was thinner in POMS patients ($P = .0432$, Table 2, Fig 1). This relationship was present in the left and right hemispheres (both $P < .05$ unadjusted, remaining significant for the left hemisphere after adjusting for multiple comparisons, Table 3), and particularly notable in the visual cortex relative to other cortical areas (Table 3, Fig 1). More detailed analyses of cortical mantle thickness, divided by brain region and hemisphere, are summarized in Table 3 and illustrated in Figures 2A–C.

When considering the visual cortex in more detail, the extrastriate areas (specifically V3 dorsal), the subregions IPS0, IPS1, and V3a in the dorsolateral visual cortex, and the ventral visual regions hV4, VO1, and FG2 demonstrated cortical thinning in POMS patients in both left and right hemispheres (all $P < .05$). Relative to controls, POMS patients demonstrated thinning of the dorsal components of the primary (V1 dorsal) and secondary (V2 dorsal)

visual cortices in the left hemisphere only (both $P < .05$, Fig 2A). Unilateral left hemisphere thinning was also noted in FEF, IPS2, FG4, and V3 ventral (all $P < .05$, Figs 2B–C). For most regions in the visual cortex, the left hemisphere was generally thinner than the corresponding region in the right hemisphere in both controls and POMS participants. In addition, the cortical thinning in the left hemisphere visual cortex in the POMS group was more pronounced, with more regions showing significant thinning compared to HCs.

Given the pivotal contribution of the fovea to visual acuity,[20] we were particularly interested in measuring the cortical region corresponding to the foveal representation. Cortical thickness in the foveal confluence did not differ between HC and POMS patients (Tables 2 and 3, Figs 1 and 2A). When the foveal confluence was subdivided into the different visual areas (V1, V2, and V3), none of the subdivisions differed in thickness between POMS and HCs.

DTI Measures

FA and MD of the optic radiations are presented in Table 2 and Figures 3A–B. Mean FA of the optic radiations was reduced ($P = .0042$) and MD increased ($P = .0056$) in POMS patients, findings that persisted in the normal-appearing WM of the optic radiations when focal T2 bright lesions were removed ($P = .0047$ and .0400, respectively). The mean FA and MD values in the lesions within the optic radiations were significantly different from the FA and MD of nonlesional optic radiations (both $P < .0001$). Total T2 lesion volume in the whole brain was 17,009 mm^3 (range, 2,016–53,146 mm^3) and within the optic radiations was 2,462 mm^3 (range, 141–7,390 mm^3).

Relationship Between the Measures

Within the POMS group, increased disease duration was associated with whole brain cortical thinning ($P = .030$). The annualized relapse rate did not predict cortical mantle thickness. Thinning of the entire visual cortical mantle (mean of the left and right hemispheres) occurred in POMS participants irrespective of ON history, and patients with ON did not have thinner visual cortices compared to POMS without ON. The average cortical mantle thickness of the visual cortex was not associated with binocular HCVA or LCLA, even after adjusting for ON history. The OCT measures did not show any significant relationship with whole brain cortical mantle thickness, visual cortical mantle thickness, or the posterior visual pathway DTI measures.

Decreased average FA of the optic radiations was associated with thinning of the visual cortex (adjusted $R_2 = .271$, $P = .017$, Fig 4A). Lesions in the optic radiations negatively impacted the optic radiation FA (adjusted $R_2 = .197$, $P = .004$), but did not predict visual cortex thickness ($P = .234$). Increased average MD in the optic radiations was associated with visual cortex thinning, although the relationship did not reach significance (adjusted $R_2 = .197$, $P = .272$, Fig 4B).

Discussion

The onset of MS during childhood leads to thinning of the cerebral cortex, with the visual cortex being particularly vulnerable. Interestingly, the foveal confluence is spared,

suggestive of selective resilience. Reduction of the nonfoveal visual cortex is associated with loss of integrity of occipital WM pathways, implicating anterograde degeneration as one mechanism contributing to the loss of cortical thickness, although we cannot exclude intracortical pathology and neuronal loss as possible contributing factors. Retrograde reduction in retinal integrity as measured by RNFL or GCL-IPL thinning did not correlate with visual cortex thinning, nor did we detect loss of retinal integrity in the absence of ON. These findings suggest that POMS patients may have early resilience to certain aspects of the more global neurodegenerative processes that characterize MS in adults.

The apparent sparing of the foveal confluence was intriguing. We hypothesize that sparing of the foveal confluence could represent evolutionarily conserved neuronal prioritization to preserve a core neurological function. Foveal sparing may also, in part, explain the lack of correlation between HCVA and LCLA and the reduced cortical mantle thickness seen in the occipital lobe in POMS patients. The reduced cortical mantle thickness in the nonfoveal regions, the extrastriate visual areas (especially V3), and the ventral visual areas in the fusiform gyrus (except fusiform area 3) is more likely to correlate with impairment in more abstract visual processing.

Our findings differ from studies in adult-onset MS. We did not find a relationship between OCT and visual cortex measures, even in patients with a history of ON. In contrast, in a cohort of 100 adult-onset MS patients (18–55 years of age, 90 with clinically isolated syndrome or relapsing-remitting MS [RRMS] phenotypes, and 10 with progressive MS), RNFL thinning was significantly related to visual cortex volume and optic radiation T1 lesion load.[5] Of note, the mean disease duration was 9 years, considerably longer than the average 3-year disease duration of our cohort. In the adult study, a 1 cm^3 reduction in occipital cortex volume was associated with a very small, .6 μm, reduction in RNFL thickness. Our study may be underpowered to detect such a small difference. In a separate cohort of 222 adult-onset MS patients (137 RRMS, 57 secondary, and 28 primary progressive MS, mean disease duration 20 years), GCL-IPL thinning, but not RNFL thinning, was related to focal thinning in the primary visual cortex, and only in patients with a prior history of ON.[4] The authors did not provide detailed data for the RRMS patients alone. None of the pediatric patients in our study had progressive MS, and when compounded by the marked difference in disease duration, it is probable that the findings in this adult study are more reflective of progressive disease. As such, it may not be biologically rational to extrapolate these findings to early relapsing-remitting MS.

Our inability to find a relationship between ON and cortical mantle thinning in the occipital lobe may relate, in part, to the near-complete visual acuity recovery of our POMS cohort. Only two MS-ON eyes in our cohort had residual visual acuity deficits. In two studies of adults with neuromyelitis optica, in which ON is often associated with severe visual loss, thinning in the parieto-visual cortex and visual cortex, most notably in the pericalcarine sulci, was demonstrated.[8,21] Interestingly, although we cannot find an overall relationship between visual acuity, or ON and the entire visual cortex, we did show thinning in these same subregions of the intraparietal sulcus (IPS0, IPS1, and IPS2) in the parieto-visual cortex. Future studies that enroll POMS patients with visual acuity deficits are required to more fully evaluate these relationships.

Although we were particularly interested in the visual cortex, we also confirmed a more global impact of POMS on cortical mantle thickness of the cerebral GM as a whole. We also noted a laterality effect. A laterality effect was also noted in a study of 250 adult MS patients and 125 HCs, where the cortical thinning in the MS group was more prominent in the left relative to the right hemisphere.[22] The biological underpinning of this finding is not clear. Conceptually, there may be greater variability in the cortical mantle thickness in the nondominant hemisphere, which could render it more difficult to detect group differences between MS and HC.

Thinning of the cerebral cortex occurred despite the young age of the POMS group and the brief disease duration. Whether thinning of the cerebral cortex predicts risk of future disability progression, as has been demonstrated in the adult-onset MS population,[10,22,23] requires longitudinal evaluation.

Given that we were evaluating POMS patients, we specifically considered whether age-expected pruning of synapses might influence measures of cortical mantle thickness. Synaptic density in the visual cortex increases to a maximum GM thickness during the first postnatal year, and then gradually decreases to a nadir at 11 years of age.[24] Synaptic density does not correlate directly with visual acuity,[25,26] but visual input to the cortex is needed for subsequent pruning of synapses.[26] Profound, early visual deprivation interrupts synaptic pruning and prevents the visual cortex from thinning, as evidenced by increased visual cortex mantle thickness in children with very early-life blindness.[27] Although the ontogeny of visual cortex maturation is an important consideration, all but one of our patients manifested with their first MS attack after 11 years of age, when normal pruning is complete. Although the preclinical phase of MS, and its duration, is unknown, and thus could conceptually have commenced at a very young age, we hypothesize that the age of onset of our patients likely had a minimal impact on normal pruning of the visual cortex.

Onset of MS during childhood and adolescence had a negative impact on cortical mantle thickness, particularly in the visual cortex. Sparing of the foveal confluence may represent a form of regional tissue resilience. The thinning of the visual cortex appears to be partly driven by loss of integrity in the optic radiations, rather than regional WM lesions. Interrogation of more complex visual processing and its relationship to cortical mantle thickness, especially the extrastriate visual cortex, is an avenue for further research.

Acknowledgments and Disclosure:

Geraldine Liu discloses her spouse’s royalties for Liu, Volpe, and Galetta’s Neuro-Ophthalmology: Diagnosis and Management, 2010, Elsevier. Brenda Banwell has received speaker honoraria and has served as a central MRI reviewer for Novartis. She also serves as a non-remunerated advisor on clinical trial design to Biogen, Sanofi, Novartis, Celgene, Roche, and Teva Neuroscience. Amy Waldman has received research support from the NIH (NINDS K23NS069806; PI; R01NS071463, site investigator), National Multiple Sclerosis Society (site PI), Biogen Idec (PI), IONIS Pharmaceutics (PI), United Leukodystrophy Foundation, and the Children’s Hospital of Philadelphia (Foerderer Award, PI), royalties from UpToDate, and served as a consultant to Optum. All other authors have nothing to disclose. This study was funded by the National Institute of Neurological Disorders and Stroke (K23NS069806, Waldman PI) and a Foerderer Award from the Children’s Hospital of Philadelphia (Waldman, PI).

References

1. Graves JS, Chohan H, Cedars B, et al. Sex differences and subclinical retinal injury in pediatric-onset MS. Mult Scler 2017;23:447–55. [PubMed: 27306618]
2. Waldman A, Ghezzi A, Bar-Or A, Mikaeloff Y, Tardieu M, Banwell B. Multiple sclerosis in children: an update on clinical diagnosis, therapeutic strategies, and research. Lancet Neurol 2014;13:936–48. [PubMed: 25142460]
3. Waldman AT, Liu GT, Lavery AM, et al. Optical coherence tomography and visual evoked potentials in pediatric MS. Neurol Neuroimmunol Neuroinflamm 2017;4:e356. [PubMed: 28626779]
4. Balk L, Steenwijk M, Tewarie P, et al. Bidirectional trans-synaptic axonal degeneration in the visual pathway in multiple sclerosis. J Neurol Neurosurg Psychiatry Res 2015;86:419–24.
5. Gabilondo I, Martínez-Lapiscina EH, Martínez-Heras E, et al. Trans-synaptic axonal degeneration in the visual pathway in multiple sclerosis. Ann Neurol 2014;75:98–107. [PubMed: 24114885]
6. Kolasinski J, Stagg CJ, Chance SA, et al. A combined post-mortem magnetic resonance imaging and quantitative histological study of multiple sclerosis pathology. Brain 2012;135:2938–51. [PubMed: 23065787]
7. Calabrese M, Seppi D, Romualdi C, et al. Gray matter pathology in MS: a 3-year longitudinal study in a pediatric population. Am J Neuroradiol 2012;33:1507–11. [PubMed: 22422186]
8. Kim SH, Kwak K, Hyun JW, et al. Widespread cortical thinning in patients with neuromyelitis optica spectrum disorder. Eur J Neurol 2016;23:1165–73. [PubMed: 27108769]
9. Sepulcre J, Goni J, Masdeu JC, et al. Contribution of white matter lesions to gray matter atrophy in multiple sclerosis: evidence from voxel-based analysis of T1 lesions in the visual pathway. Arch Neurol 2009;66:173–9. [PubMed: 19204153]
10. Sailer M, Fischl B, Salat D, et al. Focal thinning of the cerebral cortex in multiple sclerosis. Brain 2003;126:1734–44. [PubMed: 12805100]
11. Longoni G, Brown RA, Momayyezsiahkal P, et al. White matter changes in paediatric multiple sclerosis and monophasic demyelinating disorders. Brain 2017;140:1300–15. [PubMed: 28334875]
12. Polman CH, Reingold SC, Banwell B, et al. Diagnostic criteria for multiple sclerosis: 2010 revisions to the McDonald criteria. Ann Neurol 2011;69:292–302. [PubMed: 21387374]
13. Lucchinetti CF, Kiers L, O'Duffy A, et al. Risk factors for developing multiple sclerosis after childhood optic neuritis. Neurology 1997;49:1413–8. [PubMed: 9371931]
14. Tewarie P, Balk L, Costello F, et al. The OSCAR-IB consensus criteria for retinal OCT quality assessment. PLoS One 2012;7:1–7.
15. Fischl B, Dale AM. Measuring the thickness of the human cerebral cortex from magnetic resonance images. Proc Natl Acad Sci 2000;97:11050–5. [PubMed: 10984517]
16. Benson NC, Butt OH, Brainard DH, Aguirre GK. Correction of distortion in flattened representations of the cortical surface allows prediction of V1–V3 functional organization from anatomy. PLoS Comput Biol 2014;10:e1003538. [PubMed: 24676149]
17. Wang L, Mruczek REB, Arcaro MJ, Kastner S. Probabilistic maps of visual topography in human cortex. Cereb Cortex 2015;25: 3911–31. [PubMed: 25452571]
18. Rosenke M, Weiner KS, Barnett MA, et al. A cross-validated cytoarchitectonic atlas of the human ventral visual stream. Neuroimage 2017;170:257–70. [PubMed: 28213120]
19. Zeki SM. Representation of central visual fields in prestriate cortex of monkey. Brain Res 1969;14:271–91. [PubMed: 4978525]
20. Provis JM, Dubis AM, Maddess T, Carroll J. Adaptation of the central retina for high acuity vision: cones, the fovea and the avascular zone. Prog Retin Eye Res 2013;35:63–81. [PubMed: 23500068]
21. von Glehn F, Jarius S, Cavalcanti Lira RP, et al. Structural brain abnormalities are related to retinal nerve fiber layer thinning and disease duration in neuromyelitis optica spectrum disorders. Mult Scler 2014;20:1189–97. [PubMed: 24477120]
22. Narayana PA, Govindarajan KA, Goel P, et al. Regional cortical thickness in relapsing remitting multiple sclerosis: a multi-center study. NeuroImage Clin 2013;2:120–31.

23. Steenwijk MD, Geurts JJG, Daams M, et al. Cortical atrophy patterns in multiple sclerosis are non-random and clinically relevant. Brain 2016;139:115–26. [PubMed: 26637488]

24. Huttenlocher PR, de Courten C. The development of synapses in striate cortex of man. Hum Neurobiol 1987;6:1–9. [PubMed: 3583840]

25. Winfield DA. The postnatal development of synapses in the visual cortex of the cat and the effects of eyelid closure. Brain Res 1981;206:166–71. [PubMed: 7470883]

26. Bourgeois JP, Jastreboff PJ, Rakic P. Synaptogenesis in visual cortex of normal and preterm monkeys: evidence for intrinsic regulation of synaptic overproduction. Proc Natl Acad Sci 1989;86: 4297–301. [PubMed: 2726773]

27. Jiang J, Zhu W, Shi F, et al. Thick visual cortex in the early blind. J Neurosci 2009;29:2205–11. [PubMed: 19228973]

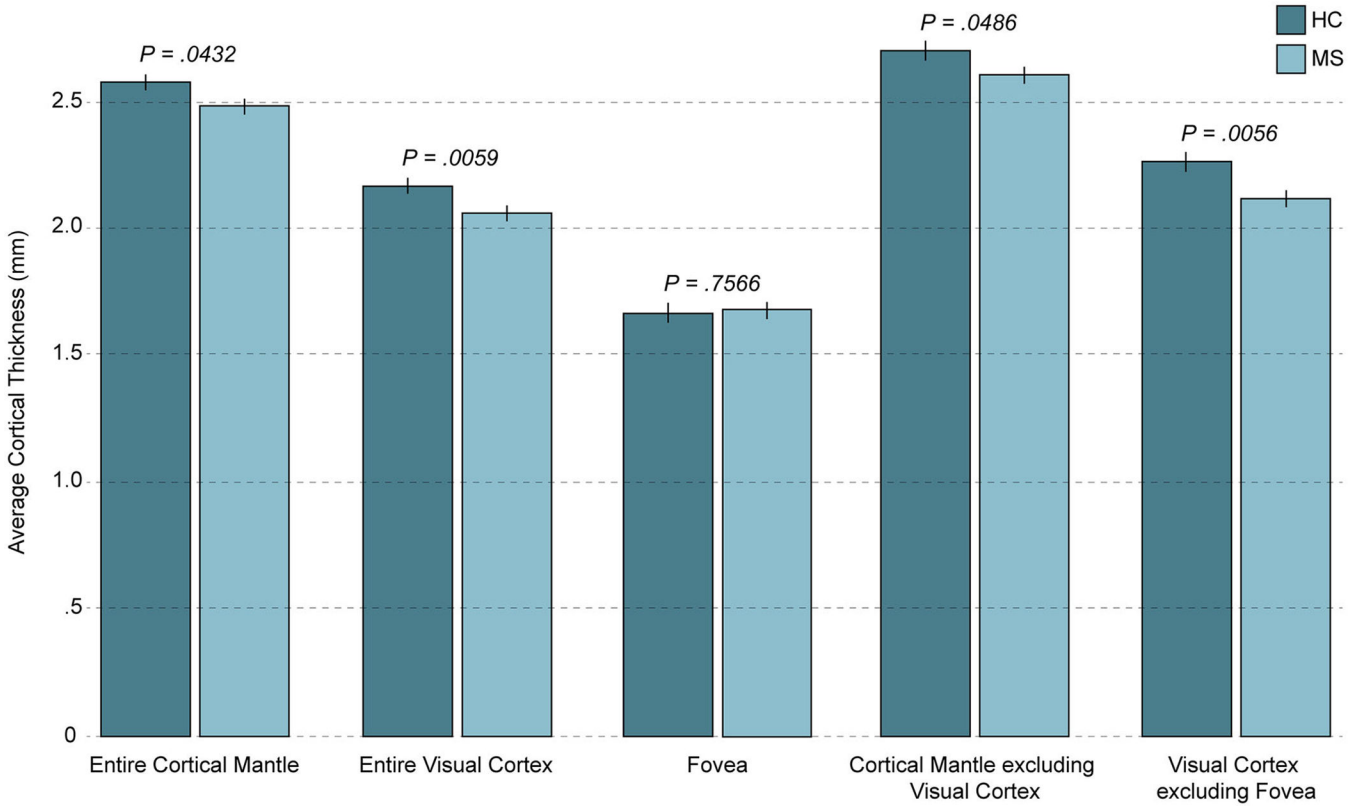

Fig 1.

Cortical mantle thickness in pediatric-onset MS and healthy controls. The average cortical thicknesses for the mean of the left and right hemispheres are shown for pediatric-onset multiple sclerosis (POMS) patients and healthy controls, and Benjamini-Hochberg adjusted *P*-values (corrected for multiple comparisons) are indicated. POMS patients demonstrated significant thinning of the entire cortical mantle, the entire visual cortex, the cortical mantle excluding the visual cortex, and the visual cortex excluding the fovea; however, the foveal confluence was spared. Thinning of the visual cortex significantly accounted for the difference between POMS patients and controls when the cortical mantle was considered as a whole. HC = healthy control; MS = multiple sclerosis.

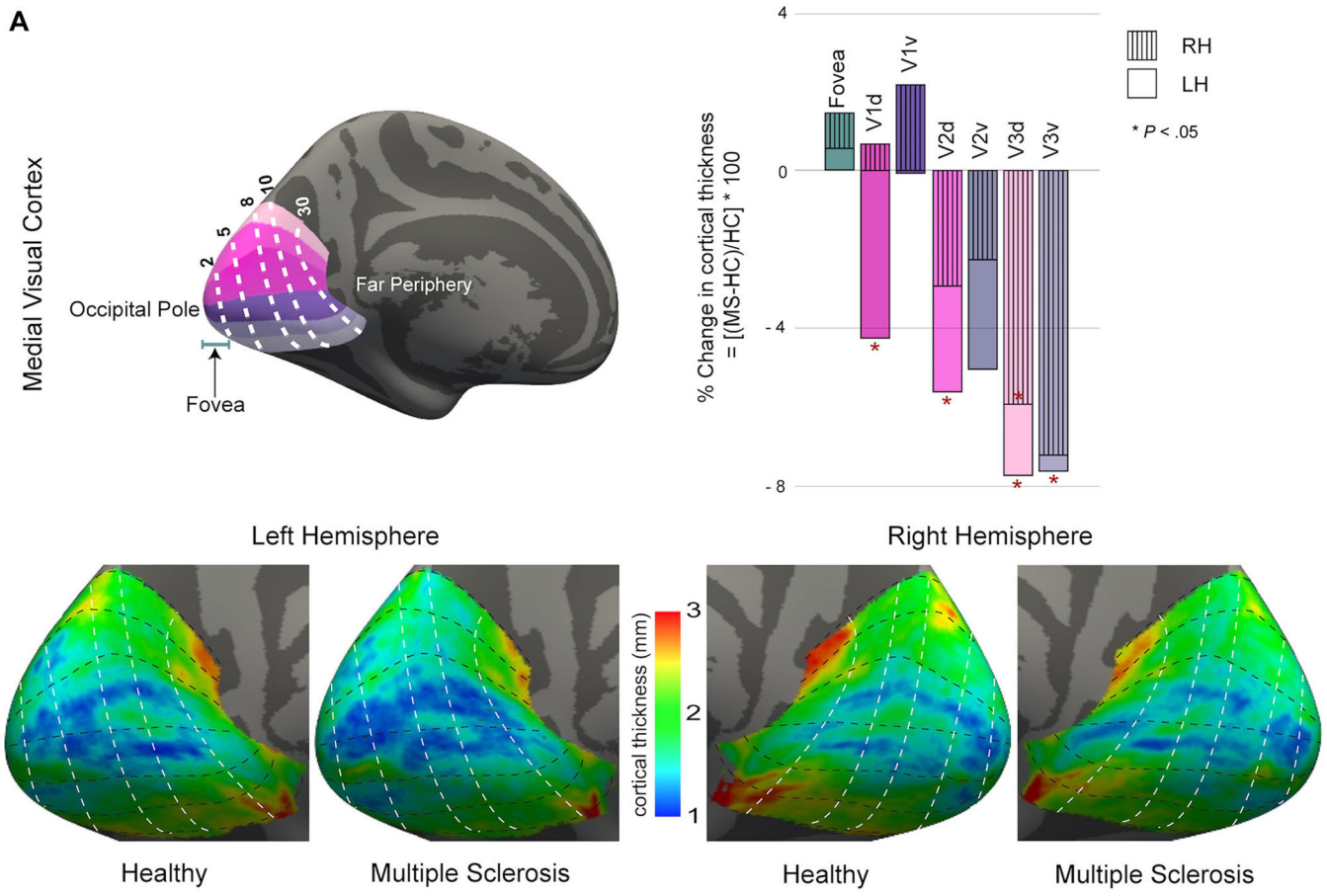

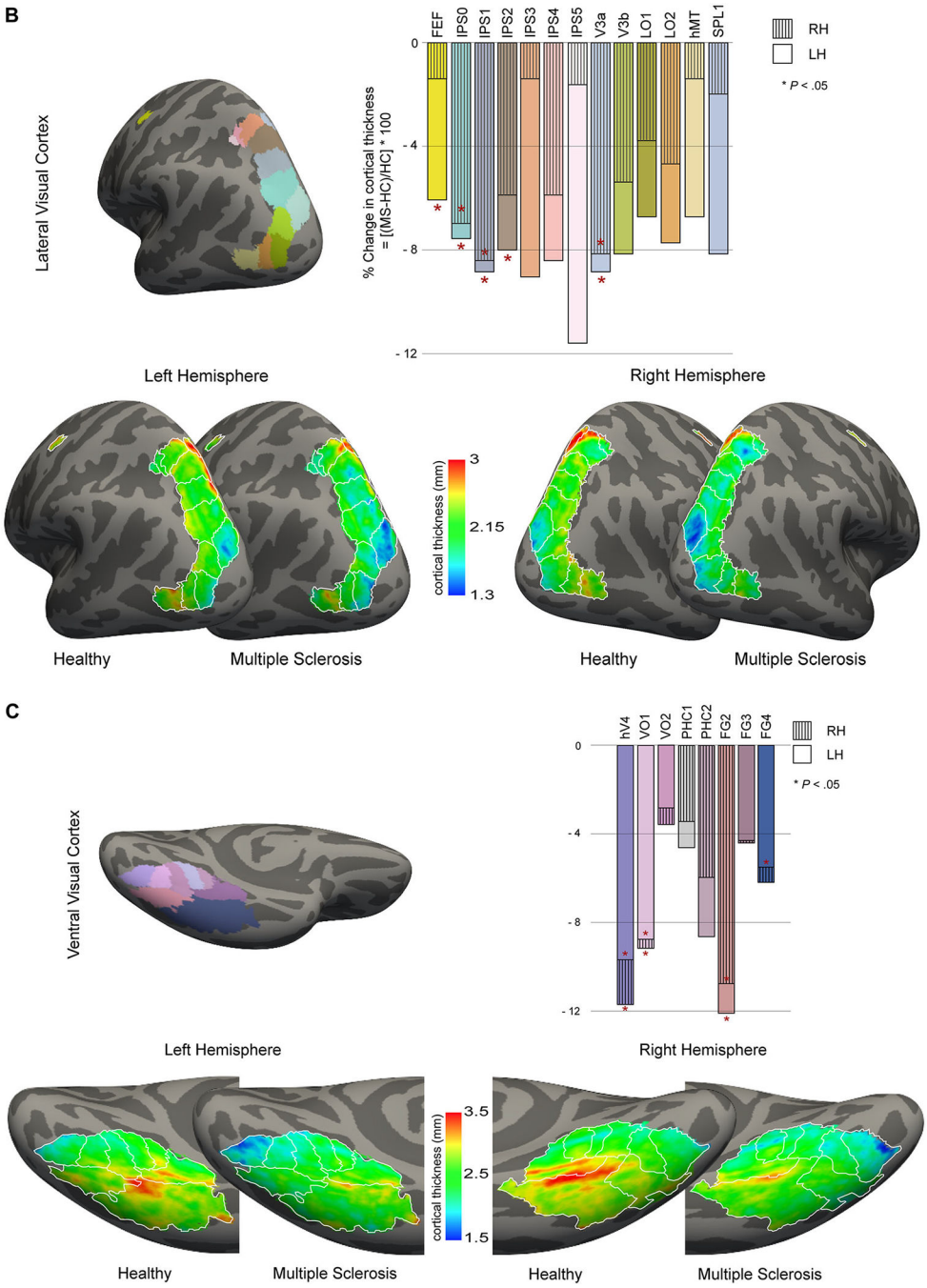

Fig 2.

Regional differences in medial (A), lateral (B), and ventral (C) visual cortical mantle thicknesses. The percentage changes in average cortical mantle thickness between pediatric-onset multiple sclerosis (POMS) subjects and healthy controls for each region of each hemisphere are shown; asterisk (*) indicates significant ($P < .05$) Benjamini-Hochberg adjust P-values (corrected for multiple comparisons). The average cortical thickness maps on the inflated surfaces of left and right hemispheres are also shown. For each panel, a common color scale has been used to compare the controls and POMS cortical thickness

maps. The red and yellow indicate thicker cortex, and blue indicates thinner cortex. RH = right hemisphere; LH = left hemisphere; HC = healthy control; MS = multiple sclerosis; hV4 = human ventral 4; VO = ventral occipital; PHC = parahippocampal cortex; FG = fusiform gyrus; V1d = primary visual cortex dorsal; V1v = primary visual cortex ventral; V2d = visual area 2 dorsal; V2v = visual area 2 ventral; V3d = visual area 3 dorsal; V3v = visual area 3 ventral; FEF = frontal eye fields; IPS = intraparietal sulcus; V3a = visual area 3a; V3b = visual area 3b; LO = lateral occipital; hMT = human middle temporal; SPL = superior parietal lobule.

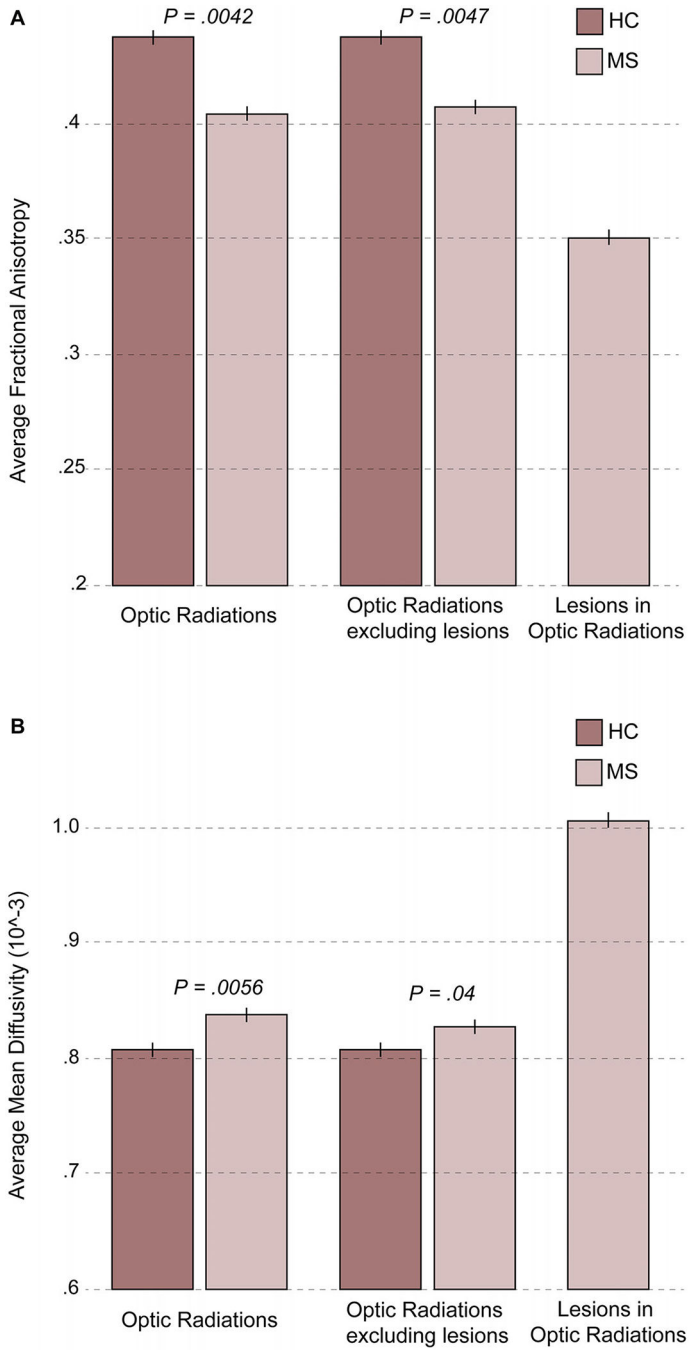

Fig 3.

(A) Fractional anisotropy in the optic radiations in pediatric-onset MS and healthy controls. In the optic radiations, average fractional anisotropy was decreased in pediatric-onset MS patients compared to healthy controls. Lesional tissue demonstrated even greater reductions in average fractional anisotropy; however, even normal appearing white matter in the optic radiations demonstrated significant changes. (B) Mean diffusivity in the optic radiations in pediatric-onset MS and healthy controls. In the optic radiations, average mean diffusivity was increased in pediatric-onset multiple sclerosis patients compared to healthy controls.

Lesional tissue demonstrated an even greater increase in average mean diffusivity; however, even normal appearing white matter in the optic radiations demonstrated significant changes. HC = healthy control; MS = multiple sclerosis.

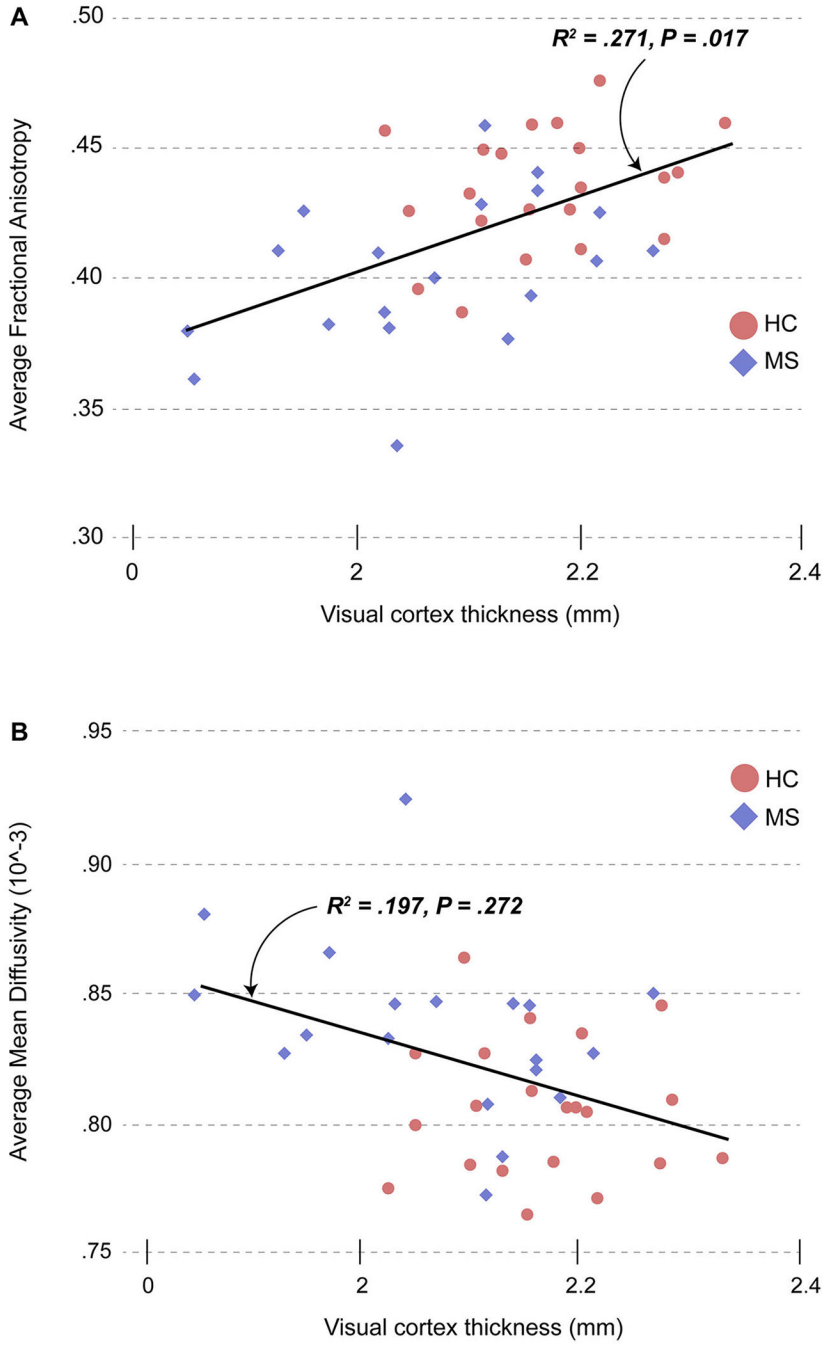

Fig 4.

(A) Relationship between fractional anisotropy in the optic radiations and visual cortical mantle thickness in pediatric-onset MS and healthy controls. Average fractional anisotropy in the optic radiations predicted visual cortex mantle thickness (mean of left and right hemispheres) after adjusting for case-control status. (B) Relationship between mean diffusivity in the optic radiations and visual cortical mantle thickness in pediatric-onset MS and healthy controls. Average mean diffusivity in the optic radiations decreased with

increasing visual cortical thickness (mean of left and right hemispheres), although the relationship did not reach significance. HC = healthy control; MS = multiple sclerosis.

Table 1.

Characteristic Features of Participants with Pediatric-Onset MS and Healthy Controls

	POMS (*N* = 20)	HC (*N* = 22)	*P*-value[a]
Age (in years) at MRI scan, mean	17.9	17.1	.4060
SD (range)	3.1 (13–24)	2.8 (12–23)	
Female:male	11:9	16:6	.2311
Disease duration (in years), mean	3.1	N/A	N/A
SD (range)	3.0 (.3–11.8)		
Total number of relapses, mean	3.7	N/A	N/A
SD (range)	2.9 (1–11)		
Annualized relapse rate, mean	1.7	N/A	N/A
SD (range)	1.3 (.3–5.3)		
Treatment at time of MRI, *N* (%)	Interferon 14 (70%) Glatiramer acetate 6 (30%)	N/A	N/A
Time (in years) of exposure to any chronic immunomodulatory therapy, mean	2.1	N/A	N/A
SD (range)	2.5 (0–8.5)		
EDSS, median (range)	1 (0–3.5)	N/A	N/A
Number with a history of optic neuritis, *N* (%)	10 (50%) (bilateral 3, right 3, and left 4)	N/A	N/A

POMS = pediatric-onset multiple sclerosis; HC = healthy control; SD = standard deviation; N/A = not applicable; EDSS = Expanded Disability Status Scale.

[a] *P*-value was determined using the Student's *t*-test for independent samples.

Table 2.

Structural and Functional Metrics in Pediatric-Onset MS Participants and Healthy Controls

	POMS	HC	*P*-value[a]	Adjusted *P*-value[b]
Visual acuity (number of letters correct)				
Binocular high-contrast visual acuity, mean (SD)	57.5 (4.3)	57.2 (6.6)	.8512	.8512
Binocular low contrast letter acuity (2.5%), mean (SD)	31.3 (9.5)	34.7 (6.8)	.1766	.2060
Binocular low contrast letter acuity (1.25%), mean (SD)	22.2 (9.2)	28.2 (7.1)	.0221	.0387
Optical coherence tomography (microns)				
Retinal nerve fiber layer thickness (averaged mean for both eyes), mean (SD)	90.7 (13.9)	98.5 (9.0)	.0343	.0480
Ganglion cell layer-inner plexiform layer thickness (averaged mean for both eyes), mean (SD)	76.1 (8.5)	83.2 (6.0)	.0046	.0107
Diffusion tensor imaging				
Fractional anisotropy of the optic radiations, mean (SD)	.40 (.02)	.43 (.02)	.0006	.0042
Fractional anisotropy of lesions within the optic radiations, mean (SD)	.35 (.03)	N/A	N/A	
Fractional anisotropy of normal-appearing white matter (non-lesional) within the optic radiations, mean (SD)	.40 (.02)	.43 (.02)	.0010	.0047
Mean diffusivity of the optic radiations, mean (SD)	.84 (.02)	.80 (.02)	.0020	.0056
Mean diffusivity of lesions within the optic radiations, mean (SD)	1.01 (.09)	N/A	N/A	
Mean diffusivity of normal-appearing white matter (non-lesional) within the optic radiations, mean (SD)	.83 (.02)	.80 (.02)	.0200	.0400
Cortical mantle thickness (mm)				
Whole brain, mean (SD)	2.49 (.13)	2.58 (.12)	.0278	.0432
Visual cortex, mean (SD)	2.07 (.12)	2.17 (.08)	.0017	.0059
Whole brain excluding visual cortex, mean (SD)	2.61 (.13)	2.70 (.15)	.0382	.0486
Fovea, mean (SD)	1.69 (.14)	1.67 (.14)	.7026	.7566
Visual cortex (without the fovea), mean (SD)	2.13 (.12)	2.26 (.11)	.0004	.0056

[a] *P*-value was determined using the Student's *t*-test for independent samples.

[b] Benjamini-Hochberg *P*-value adjusted for multiple comparisons.

POMS = pediatric-onset multiple sclerosis; HC = healthy control; SD = standard deviation.

Table 3.

Mean Cortical Thickness (in mm) after Adjusting for Age and Sex

		Left hemisphere					Right hemisphere					Left and right hemisphere mean				
Region of interest		**HC**	**MS**	***P*-value[a]**	**Adjusted *P*-value[b]**	**%[c]**	**HC**	**MS**	***P*-value[a]**	**Adjusted *P*-value[b]**	**%[c]**	**HC**	**MS**	***P*-value[a]**	**Adjusted *P*-value[b]**	**%[c]**
Whole brain		2.58	2.48	.0174	.0473	3.94	2.58	2.49	.0304	.0713	3.31	2.58	2.49	.0278	.0432[d]	3.63
Visual cortex		2.16	2.05	.0013	.0221	4.9	2.18	2.08	.0049	.0278	4.67	2.17	2.07	.0017	.0059[d]	4.79
Whole brain excluding visual cortex		2.71	2.61	.0363	.0796	3.65	2.70	2.61	.0514	.0999	3.28	2.70	2.61	.0382	.0486[d]	3.46
Medial visual cortex	Fovea	1.67	1.68	.8551	.8679	−.55	1.67	1.70	.6327	.7171	−1.44	1.67	1.69	.7026	.7566[d]	−1.00
	V1	1.55	1.52	.1504	.2273	2.20	1.63	1.66	.5028	.5895	−1.43	1.59	1.59	.8236	.8236	.33
	V1 dorsal	1.59	1.53	.0137	.0405	4.22	1.63	1.64	.7847	.8209	−.67	1.61	1.58	.2782	.2981	1.75
	V1 ventral	1.51	1.51	.9763	.9763	.07	1.63	1.67	.3881	.4887	−2.19	1.57	1.59	.5984	.6190	−1.11
	V2	1.82	1.72	.0066	.0281	5.32	1.97	1.92	.3164	.4059	2.59	1.89	1.82	.0638	.1126	3.90
	V2 dorsal	1.85	1.75	.0061	.0296	5.62	1.92	1.87	.2425	.3298	2.96	1.89	1.81	.0275	.0635	4.26
	V2 ventral	1.78	1.69	.0743	.1295	5.02	2.01	1.97	.5262	.6065	2.24	1.9	1.83	.2216	.2659	3.55
	V3	2.09	1.93	.0002	.0068	7.65	2.17	2.03	.0050	.0262	6.57	2.13	1.98	.0006	.0045	7.10
	V3 dorsal	2.02	1.87	.0001	.0068	7.70	2.03	1.91	.0071	.0268	5.88	2.03	1.89	.0002	.0060	6.79
	V3 ventral	2.15	1.98	.0035	.0238	7.60	2.31	2.15	.0310	.0703	7.17	2.23	2.06	.0078	.0213	7.38
Lateral visual cortex	FEF	2.54	2.39	.0031	.0264	6.05	2.56	2.52	.6458	.7199	1.40	2.55	2.45	.1213	.1915	3.72
	IPS0	2.23	2.08	.0017	.0231	6.88	2.23	2.06	.0075	.0268	7.52	2.23	2.07	.0013	.0078	7.20
	IPS1	2.27	2.08	.0020	.0227	8.34	2.23	2.03	.0069	.0276	8.84	2.25	2.05	.0019	.0095	8.59
	IPS2	2.41	2.22	.0082	.0279	7.95	2.28	2.15	.0814	.1384	5.79	2.35	2.18	.0063	.0210	6.90
	IPS3	2.35	2.32	.7633	.8110	1.26	2.23	.203	.0219	.0552	9.05	2.29	2.17	.1401	.2001	5.05
	IPS4	2.08	1.96	.2260	.3136	5.82	2.18	2.00	.0554	.1018	8.24	2.13	1.98	.0755	.1258	7.06
	IPS5	1.95	1.92	.8471	.8728	1.35	2.46	2.18	.0950	.1538	11.53	2.21	2.05	.1729	.2358	7.03
	V3a	1.91	1.75	.0042	.0260	8.10	1.94	1.77	.0030	.0291	8.73	1.92	1.76	.0005	.0050	8.42
	V3b	2.23	2.05	.0498	.1026	8.04	2.14	2.03	.1558	.2303	5.35	2.19	2.04	.0397	.0851	6.72
	LO1	2.00	1.92	.2180	.3088	3.78	2.10	1.95	.0502	.1004	6.75	2.05	1.94	.0525	.0984	5.30
	LO2	2.28	2.17	.1605	.2322	4.56	2.32	2.14	.0465	.0988	7.76	2.30	2.16	.0135	.0338	6.18
	hMT	2.40	2.37	.6520	.7151	1.32	2.40	2.23	.0524	.0990	6.73	2.40	2.30	.1314	.1971	4.02
	SPL1	2.73	2.67	.6811	.7352	2.09	2.81	2.59	.0910	.1509	8.14	2.77	2.63	.2031	.2539	5.16

Region of interest		Left hemisphere					Right hemisphere					Left and right hemisphere mean				
		HC	MS	*P*-value[a]	Adjusted *P*-value[b]	%[c]	HC	MS	*P*-value[a]	Adjusted *P*-value[b]	%[c]	HC	MS	*P*-value[a]	Adjusted *P*-value[b]	%[c]
Ventral visual cortex	hV4	2.22	2.01	.0061	.0277	9.67	2.29	2.03	.0083	.0269	11.70	2.26	2.02	.0026	.0111	10.70
	VO1	2.45	2.23	.0140	.0397	8.77	2.45	2.23	.0111	.0343	9.15	2.45	2.23	.0035	.0131	8.96
	VO2	2.40	2.33	.3941	.4786	2.80	2.44	2.35	.3123	.4164	3.52	2.42	2.34	.2778	.3205	3.16
	PHC1	2.46	2.35	.1155	.1785	4.52	2.37	2.29	.4186	.4994	3.39	2.42	2.32	.1849	.2412	3.96
	PHC2	2.66	2.43	.3941	.4873	2.80	2.44	2.35	.3123	.4084	3.52	2.42	2.34	.2778	.3087	3.16
	FG2	2.73	2.40	.0005	.0113	12.09	2.74	2.44	.0033	.0249	10.76	2.74	2.42	.0003	.0045	11.43
	FG3	2.60	2.49	.0579	.1036	4.30	2.60	2.49	.1061	.1678	4.38	2.60	2.49	.0459	.0918	4.34
	FG4	2.74	2.59	.0186	.0486	5.50	2.88	2.70	.0229	.0556	6.22	2.81	2.64	.0074	.0222	5.87

[a] *P*-value was determined using the Student's *t*-test for independent samples.

[b] Benjamini-Hochberg *P*-value adjusted for multiple comparisons. *P*-values comparing POMS and HC for left hemisphere and right hemisphere were grouped and adjusted separately from the *P*-values comparing POMS and HC for the mean of the left and right hemispheres (ie, two independent false discovery rate calculations were performed).

[c] Percentage of cortical thinning in the region among MS patients compared to healthy controls.

[d] *P*-values were previously adjusted as part of the Table 2 false discovery rate calculation; the *P*-values from Table 2 are reported here.

POMS = pediatric-onset multiple sclerosis; HC = healthy control; V1 = primary visual cortex; V2 = visual area 2; V3 = visual area 3; FEF = frontal eye fields; IPS = intraparietal sulcus; LO = lateral occipital; hMT = human middle temporal; SPL = superior parietal lobule; hV4 = human ventral 4; VO = ventral occipital; PHC = parahippocampal cortex; FG = fusiform gyrus.